Fictive-impurity approach to dynamical mean-field theory: A strong-coupling investigation

A. Fuhrmann,[1] S. Okamoto,[2] H. Monien,[1] and A. J. Millis[2]
[1]*Physikalisches Institut, Universität Bonn, Nußallee 12, D-53115 Bonn, Germany*
[2]*Department of Physics, Columbia University, 538 West 120th Street, New York, New York 10027, USA*
(Received 11 December 2006; revised manuscript received 22 February 2007; published 21 May 2007)

Quantum Monte Carlo and semiclassical methods are used to solve two- and four-site cluster dynamical mean-field approximations to the square-lattice Hubbard model at half filling and strong coupling. The dyanmical cluster approximation, cluster dynamical mean-field theory, and fictive-impurity approaches are compared. The energy, spin correlation function, phase boundary, and electron spectral function are computed and compared to available exact results. The comparision permits a quantitative assessment of the ability of the different methods to capture the effects of intersite spin correlations. Two real-space methods and one momentum-space representation are investigated. One of the two real-space methods is found to be significantly worse: in it, convergence to the correct results is found to be slow and, for the spectral function, nonuniform in frequency, with unphysical midgap states appearing. Analytical arguments are presented showing that the discrepancy arises because the method does not respect the pole structure of the self-energy of the insulator. Of the other two methods, the momentum-space representation is found to provide the better approximation to the intersite terms in the energy but neither approximation is particularly acccurate and the convergence of the momentum-space method is not uniform. A few remarks on numerical methods are made.

DOI: 10.1103/PhysRevB.75.205118 PACS number(s): 71.10.Fd, 75.10.−b

I. INTRODUCTION

"Strongly correlated" materials[1] pose one of the outstanding challenges in condensed matter physics. These materials exhibit a wide range of interesting and potentially useful properties including high-temperature superconductivity[2] and magnetism with very high spin polarization;[3] however, in these classes of material the electron-electron and electron-lattice interactions are so strong that the conventional approach (using density functional theory to compute bands and then using perturbative methods to treat residual interactions between quasiparticles) fails. Developing a reliable, material-specific theoretical framework for determining the behavior of strongly correlated compounds is an outstanding challenge to materials theory.

The development of single-site dynamical mean-field theory[4] was a fundamental step forward in correlated electron science. In this approach one approximates the momentum- and frequency-dependent self-energy $\Sigma(p,\omega)$ by a momentum-independent function $\Sigma(p,\omega)\rightarrow\Sigma(\omega)$. This approximation allows the construction of a *nonperturbative* and computationally tractable theoretical procedure for computing physical properties: because it is a function of only one frequency variable, the self-energy may be viewed as the self-energy of a single-site "quantum-impurity model," with the parameters of the model specified by a self-consistency condition. The approach works very well for situations (including the Mott transition in electronically three-dimensional materials,[5] the "double-exchange" physics important for colossal magentoresistance manganites,[6] and the basic physics of heavy-fermion compounds[7]), in which Galilean invariance is strongly broken and the dominant physics is on site. However, in wide classes of interesting materials, intersite correlations play an important role in physics. Examples include the high-temperature superconductors, where the predictions of the single-site dynamical mean-field theory have been shown to disagree strongly with data on the evolution with doping of quasiparticle velocity and "Drude" optical weight[8] and the orbital order and polaron glass physics of the manganites.[9] Extension of the dynamical mean-field method to include intersite correlations is therefore an important issue.

The single-site dynamical mean-field theory involves the mapping of a lattice model onto a single-site quantum impurity model. A natural extension is to consider a multisite impurity model ("cluster"), whose various self-energies could be used to obtain a better representation of the lattice self-energy. Several proposals have been made including a self-consistent embedding of a physical cluster [cluster dynamical mean-field theory[10] (CDMFT)] and a momentum-space approximation [dynamical cluster approximation (DCA)].[11] Recently a unifying fictive-impurity (FI) picture was presented,[12,13] in which the different approaches were seen to correspond to different choices of basis in the same general expansion for the self-energy.

The relative merits of the different approaches have been debated,[15] but there have been relatively few comparisions of the different methods in the relevant physical limits. In this paper we take a step towards remedying this deficiency by presenting, for the two-dimensional (2D) half-filled Hubbard model in the strong-correlation limit, a numerical study of real-space and momentum-space cluster dynamical mean-field algorithms along with a comparison to analytics. A feature of our analysis is that we are able to identify the contributions which arise from true intersite correlations (i.e., those not occurring in the single-site approximation) and compare them to exact (high-temperature series) results, thereby quantifying the degree to which the different methods capture the intersite correlations.

Our results reveal that none of the methods give a particularly good treatment of the intersite correlations The real-space method discussed in Ref. 12 has severe inadequacies, which arise mathematically from an incorrect treatment of the pole structure of the self-energy. The importance of re-

specting the pole structure of the self-energy was recently stressed by Stanescu and Kotliar.[14] Our results also point to a fundamental deficiency of the fictive-impurity-model approach (in any of its implementations): while general arguments[12,13] guarantee that *some* cluster model exists which reproduces any given approximation to a lattice model, the construction of the cluster model (in particular the choice of interaction terms) is not a trivial issue. While the DCA[11] provides a better approximation to the intersite contributions than do the other methods,[10,12,13] none of the approaches are particularly accurate. We suggest that an impurity model with additional interaction terms would likely be superior.

The rest of this paper is organized as follows: Section II defines the formalism we use and presents a few remarks on issues related to numerical implementations. Section III presents our numerical results. Section IV gives analytical arguments which shed light on some of the findings, and Sec. V is a conclusion.

II. FORMALISM

A. General aspects

A general result of many-body theory is that all electronic physics of a given system can be obtained from the "Luttinger-Ward functional"[16] Φ of the electronic self-energy $\Sigma(p,\omega)$:

$$\Phi = \Omega_{skel}(\sigma) - \mathrm{Tr}\ \ln[\mathcal{G}_0^{-1} - \Sigma]. \tag{1}$$

Here $\mathcal{G}_0=(\partial_t-\hat{H}_0)^{-1}$ is the Green function of the associated noninteracting model and the Luttinger-Ward functional Ω_{skel} is defined as the sum of all vacuum-to-vacuum skeleton diagrams (with appropriate symmetry factors) and is here viewed as a functional of the electronic self-energy. The physical self-energy corresponding to a given noninteracting problem (specified by $\mathcal{G}_0$) is determined from the stationarity condition

$$\frac{\delta\Phi}{\delta\Sigma(p,\omega)} = 0, \tag{2}$$

which follows because Ω_{skel} has the property that

$$\frac{\delta\Omega_{skel}}{\delta\Sigma(p,\omega)} = G(p,\omega). \tag{3}$$

The situation is closely analogous to that obtaining in density functional theory, where general theorems[17] guarantee the existence of a functional of the electron density, which is the sum of a system-specific part and a universal part, is minimized at the physical density, and from which the ground-state energy can be calculated. Density functional theory became a useful tool following the demonstration of Kohn and Sham[18] that uncontrolled but reasonably accurate approximations to the universal function could be constructed and that a relatively convenient procedure for performing the minimization could be found. Similarly, new progress in many-body physics has become possible following the formulation of an uncontrolled but reasonably accurate approximation to Ω_{skel} along with a procedure for performing the minimization. The approximation $\Sigma(p,\omega) \rightarrow \Sigma(\omega)$ (analogous to the local density approximation) was shown[4,19] to permit the calculation of Ω_{skel} in terms of the solution of a quantum-impurity model with parameters fixed by the stationarity condition, Eq. (2).

The possibility of extending the approach to capture some part of the momentum dependence was alluded to in early work.[4] A discussion was given in previous work by some of us[12] (see also closely related work of Potthoff[13]). In this paper we present detailed studies using the formulation of Ref. 12. To establish the notation and define clearly the assumptions made, we outline the results of Ref. 12 here. First, one approximates the momentum dependence of the self-energy in terms of a finite number N of basis functions $\phi_j(p)$,

$$\Sigma(p,\omega) \rightarrow \Sigma_{approx}(p,\omega) \equiv \sum_{i=0}^{N-1} \phi_j(p)\Sigma_j(\omega), \tag{4}$$

such that as $N\rightarrow\infty$, $\Sigma_{approx}\rightarrow\Sigma(p,\omega)$. If one substitutes Eq. (4) into Eq. (1), one obtains a functional Φ_{approx} of N self-energy functionals Σ_j. The stationarity condition, Eq. (2), becomes the dynamical mean-field self-consistency condition

$$\frac{\delta\Phi_{approx}}{\delta\Sigma_j(\omega)} = G_{imp}(\omega) = \int \frac{d^d p}{(2\pi)^d}\phi_j(p)[\mathcal{G}_0^{-1}(p,\omega) - \Sigma_{approx}(p,\omega)]^{-1}. \tag{5}$$

The most general such functional Φ_{approx} is an N-site quantum-impurity model, which should be regarded simply as a machine for computing the N functions $\Sigma_j(\omega)$ needed to generate the approximation for $\Sigma(p,\omega)$. The impurity model need not be a physical subcluster of the original lattice and is therefore referred to as "fictive."

Specifying the impurity model is not a trivial issue. The usual procedure is to *assume* that it is given by the action

$$S_{imp} = \int d\tau d\tau' \mathbf{a}_{ij}(\tau-\tau')\psi_i^\dagger(\tau')\psi_j(\tau) + H_{int}, \tag{6}$$

where H_{int} is exactly the interaction terms of the original lattice and the $\mathbf{a}_{ij}$ are mean-field functions to be determined from the self-consistency equation. The impurity model is then some sort of self-consistently embedded subcluster of the lattice model. Interactions extending outside the cluster are neglected.

Reference[12] showed that the different cluster dynamical mean-field schemes proposed in the literature are all variants of this general scheme, with the differences arising from different choices of basis function $\phi_j(p)$. However, while it is clear that as $N\rightarrow\infty$ the procedure converges to the full solution of the lattice problem, it is not clear that at any finite N the impurity-model ansatz, Eq. (6), generates the functional Φ which would be obtained by replacing $\Sigma(p,\omega)$ by $\Sigma_{approx}(p,\omega)$ in Ω_{skel} above. As we discuss in more detail in the Conclusions, one interpretation of the results we present

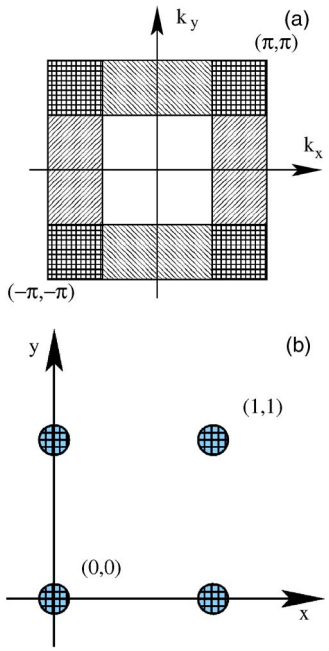

FIG. 1. (Color online) Upper panel: Brillouin zone partition corresponding to four-site dynamical cluster approximation. The zone is partitioned into four tiles: a tile centered at momentum (0,0) (unshaded), one centered at momentum (π,π) (dark shading), and two at momenta $(0,\pi)$ and $(\pi,0)$. Use has been made of invariance under translations by integer multiples of 2π. Lower panel: real-space structure of the corresponding cluster model

is precisely that the ansatz, Eq. (6), is not adequate.

B. Models and approximations

For our specific computations we study the Hubbard model with nearest-neighbor hopping on a two-dimensional square lattice, make two- and four-site approximations, and consider three choices of basis function ϕ_p. The first is the dynamical cluster approximation, introduced by Hettler and co-workers.[11] In the present language the DCA corresponds to partitioning the Brillouin zone into a finite number of regular tiles (square, for the two-dimensional square lattice we consider here) labeled by the momentum $\vec{P}_j$ at the center of the tile and choosing the basis functions $\phi_j(p)$ to be equal to unity if p is within the tile centered on $\vec{P}_j$ and zero otherwise. The partitioning for the four-site approximation is shown as the upper panel in Fig. 1. The result is a piecewise constant lattice self-energy specified by the functions $\Sigma_{\vec{P}_j}(\omega)$ giving the value of the self-energy in each Brillouin zone region, thus

$$\Sigma^{DCA}(p,\omega) = \sum_{\vec{P}_j} \phi_{\vec{P}_j}(p)\Sigma_{\vec{P}_j}(\omega). \tag{7}$$

The corresponding impurity model is the four-site cluster shown in the lower panel of Fig. 1. This cluster has four self-energies, corresponding to the on-site, first-neighbor, and second-neighbor separations; these are related to the $\Sigma_{\vec{P}_j}$ via

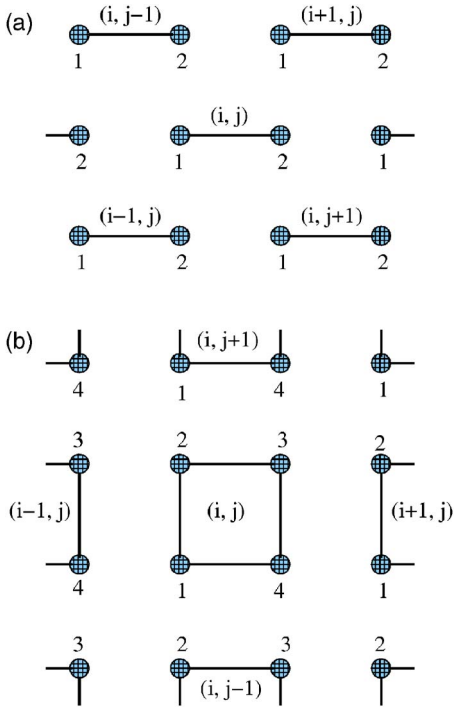

FIG. 2. (Color online) Panel (a): possible partitioning of the 2D square lattice for two-site CDMFT. Panel (b): possible partitioning of the 2D square lattice for four-site CDMFT

$$\Sigma((0,0),\omega) = \Sigma_0(\omega) + 2\Sigma_1(\omega) + \Sigma_2(\omega),$$

$$\Sigma((\pi,0),\omega) = \Sigma((0,\pi),\omega) = \Sigma_0(\omega) - \Sigma_2(\omega),$$

$$\Sigma((\pi,\pi),\omega) = \Sigma_0(\omega) - 2\Sigma_1(\omega) + \Sigma_2(\omega). \tag{8}$$

The second choice of basis function is the CDMFT approach introduced by Kotliar and co-workers.[10] In this approach one partitions the real-space lattice into a period array of regular placquettes (supercells), as shown in Fig. 2, so that the Hamiltonian becomes $H=H_{plac}+\mathbf{T}$ with $H_{plac}=H^0_{pl}+H_{int}$ an impurity model defined by the hoppings and interactions on the placquette and $\mathbf{T}$ the interplacquette hopping. The cluster is treated as an impurity and is solved, leading to a self-energy $\mathbf{\Sigma}$ which is a matrix in the space defined by the cluster. The lattice Green function is $\mathbf{G}^{-1}=\omega-\mathbf{E}(p)-\mathbf{\Sigma}$ with $\mathbf{E}(p)=H^0_{pl}+\mathbf{T}(p)$.

The CDMFT approximation necessarily breaks some of the lattice symmetries. In the two-site approximation both point-group and translational symmetries are broken. Various choices are possible. For the choice displayed in Fig. 2 the unit cell is chosen so that the primitive translation vectors are $\hat{\mathbf{u}}=\hat{\mathbf{x}}+\hat{\mathbf{y}}$ and $\hat{\mathbf{v}}=\hat{\mathbf{x}}-\hat{\mathbf{y}}$. Indexing $\hat{\mathbf{u}}$ by i and $\hat{\mathbf{v}}$ by j we have

$$H^0_{pl} = -t\begin{pmatrix} 0 & 1 \\ 1 & 0 \end{pmatrix}, \tag{9}$$

while the interplacquette hopping connects, say, site 2 on placquette (i,j) to sites 1 on placquettes $(i+1,j)$, $(i,j+1)$, and $(i+1,j+1)$, so that after Fourier transformation,

$$\mathbf{E}(p) = -t\begin{pmatrix} 0 & \psi(p) \\ \psi(p)^* & 0 \end{pmatrix}, \tag{10}$$

with $\psi(p)=1+e^{i\sqrt{2}p_u}+e^{i\sqrt{2}p_v}+e^{i\sqrt{2}(p_u+p_v)}$ and p_u, p_v vectors perpendicular to v and u, respectively. In the four-site CDMFT method,

$$H^0_{pl} = -t\begin{bmatrix} 0 & 1 & 0 & 1 \\ 1 & 0 & 1 & 0 \\ 0 & 1 & 0 & 1 \\ 1 & 0 & 1 & 0 \end{bmatrix}, \tag{11}$$

while the interplacquette hopping connects, say, site 1 on placquette (i,j) to site 2 on placquette $(i,j-1)$ and to site 4 on placquette $(i-1,j)$, so that after Fourier transformation,

$$\mathbf{E}(p) = -t\begin{bmatrix} 0 & 1+e^{2ip_y} & 0 & 1+e^{2ip_x} \\ 1+e^{-2ip_y} & 0 & 1+e^{2ip_x} & 0 \\ 0 & 1+e^{-2ip_x} & 0 & 1+e^{-2ip_y} \\ 1+e^{-2ip_x} & 0 & 1+e^{2ip_y} & 0 \end{bmatrix}. \tag{12}$$

A third choice of basis function arises from a more straightforward real-space expansion: $\Sigma(\mathbf{R},\omega)\rightarrow\Sigma(\mathbf{R}=0,\omega)+\Sigma_{\mathbf{a}}\Sigma(\mathbf{a},\omega)+\cdots$ with $\mathbf{a}$ the set of vectors connecting a site to its neighbors. For historical reasons we refer to this as the (real-space) FI method. Retaining only a few terms in this sum leads to a momentum-space self-energy expanded in the standard orthogonal harmonic functions. For example, if only on-site and nearest-neighbor terms are retained, then a d-dimensional cubic lattice would lead to a $(2d+1)$-site impurity model which could be solved to specify the quantities $\Sigma_0,\Sigma_{\hat{x}},\ldots$. However, if the point-group symmetry is unbroken, then many of the self-energies are equal and one should be able to obtain the self-energies from a smaller impurity model (two site, if only nearest-neighbor terms are retained; four site if first- and second-neighor terms are retained). Defining, for the two-dimensional case,

$$\gamma_p^{(1)} \equiv \gamma_p = \frac{1}{2}\{\cos(p_x)+\cos(p_y)\}, \tag{13}$$

$$\gamma_p^{(2)} = \cos(p_x)\cos(p_y), \tag{14}$$

we write the self-energy for the two-site cluster as

$$\Sigma(\mathbf{p},\omega) = \Sigma_0 + 4\gamma_p\Sigma_1(\omega) \tag{15}$$

and for the four-site cluster as

$$\Sigma(\mathbf{p},\omega) = \Sigma_0 + 4\gamma_p^{(1)}\Sigma_1(\omega) + 4\gamma_p^{(2)}\Sigma_2(\omega). \tag{16}$$

In the four-site case the cluster model to be solved again has the topology shown in the lower panel of Fig. 1.

C. Numerical techniques

We used two numerical techniques to solve the N-quantum impurity problem: the quantum Monte Carlo (QMC) technique using the Hirsch-Fye algorithm[4,20,21] and a recently formulated[23] semiclassical approximation.

The QMC technique is standard, but one technical issue requires comment. This method is formulated in imaginary time and involves discretization so that the imaginary time-integrations in Eq. (6) are approximated as the sum over the L "time slices" $\tau_n=n\beta/L$. The computation time scales as L^3, so the number of time slices which can be taken is limited, and at lower temperatures (larger β) the time step $\Delta\tau=\beta/L$ becomes uncomfortably large. The self-consistency step requires frequency-space information and hence a Fourier transform which becomes inaccurate above the "Nyquist frequency" $\omega_N=\pi L/\beta$. An additional difficulty is that the Green function has magnitude and derivative discontinuities across $\tau=0$ (corresponding to power-law decay at high frequencies); these must be represented accurately to obtain the high-frequency behavior correctly. Doing so is difficult because in the strong-interaction limit G varies rapidly near $\Delta\tau=0$. Thus, the errors at frequencies of the order of the Nyquist frequency are large and for the range of L accessible to us the resulting errors are too large to yield reasonable estimates of the Green function.

To mitigate the problems one must incorporate *a priori* information about the short-time behavior of the Green function into the analysis by using the short-time expansion of the equation of motion for the lattice Green function to fix the size of the magnitude and derivative discontinuities across $\tau=0$. This is typically done via the following trick:[24] one introduces a "model function" $G_{model}(\tau-\tau')$ which has the correct high-frequency behavior up to some order ω^{-m} and considers the difference $\delta G(\tau)$ between the model function and the QMC data. The low-frequency behavior of the model function is not important; we took the appropriate momentum integrals of the lattice Green function with the self-energy $\Sigma_\sigma(\omega)=U(n_{-\sigma}-0.5)+U^2n_{-\sigma}(1-n_{-\sigma})/\omega$. The difference function δG is by assumption smooth near $\tau=0$, and in particular the first $m-1$ derivatives are continuous. In practice a reasonable choice of model function leads to a δG which varies much less rapidly near $\tau=0$ than the original data or the actual Green function.

By taking the difference between the QMC data and the model function, one obtains an approximation to δG at the discrete points $\tau_n=n\beta/L$. One includes the *a priori* information concerning the high-frequency behavior by performing an order-m spline fit assuming that across $\tau=0$ the first $m-1$ derivatives are continuous. In the single-site DMFT a cubic spline was found to be sufficient[24] but in our investigations of multisite models it was found necessary to fix the ω^{-4} behavior of the Green function in order to control the high-frequency behavior of the first-neighbor self-energy. This necessitated the use of a fourth-order spline fit to the QMC data. Figure 3 demonstrates this effect, comparing the results of three different computations of the on-site self-energy using a two-site cluster (in the real-space formulation) to the known high-frequency behavior.

Obtaining real-frequency information from QMC calculations requires analytical continuation. To obtain the results presented in this paper we used a program written by Assaad,[22] with a model function corresponding to a flat density of states.

The QMC method remains very computationally expensive; one requires a time slice short enough that $U\Delta\tau\lesssim 1$ and

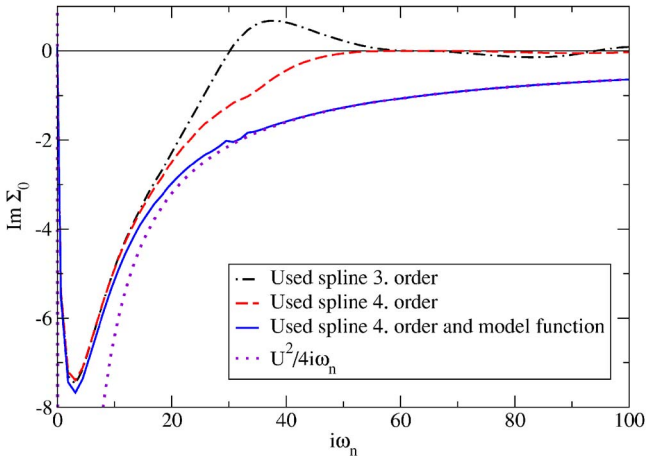

FIG. 3. (Color online) Two-site cluster approximation to the frequency-dependent on-site self-energy for the paramagnetic phase of a two-dimensional Hubbard model with $U/t=16$ at temperature $T/t=0.2$ calculated by standard procedure (third-order spline fit, dash-dotted line), and fourth-order spline fit directly to QMC data (dashed line), and fourth-order spline fit plus model function subtraction (solid line). [The model function was obtained by appropriate integral of lattice Green function with $\Sigma_\sigma(\omega)=U(n_{-\sigma}-0.5)+U^2n_{-\sigma}(1-n_{-\sigma})/\omega$.] Results are compared to the exact leading analytical high-frequency result (dotted line).

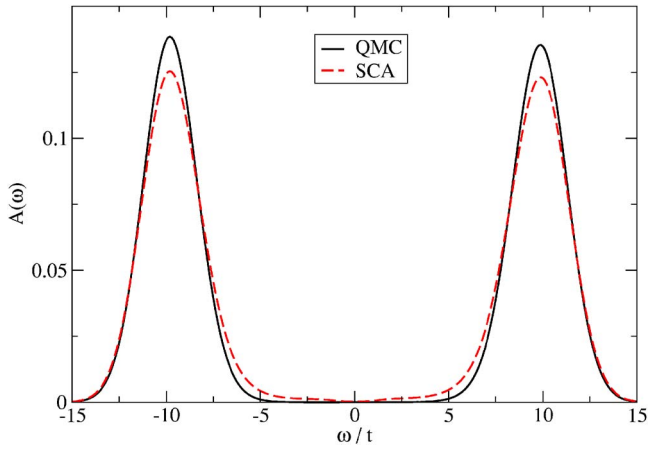

FIG. 4. (Color online) Single-impurity DMFT results for the spectral function $A_0=-\frac{1}{\pi}\,\mathrm{Im}\,G_0$ computed by the QMC and SCA methods. Solid line is the QMC and dashed line is the SCA result. $U/t=20$ and $T/t=0.5$.

very good statistical accuracy in the computed G's. To access a wider range of parameters we also used a semiclassical approximation (SCA) we have recently developed which is much less computationally expensive. The SCA method is described in detail elsewhere,[23] so we mention here only a few aspects relevant to its implementation in the present case.

For an N-site impurity model the partition function is defined as a functional integral over the $2N$-component spin- and site-dependent spinor fields $c^\dagger$ and c as

$$Z=\int \mathcal{D}[c_j^\dagger c_j]e^{-S_{eff}}, \tag{17}$$

where

$$S_{eff}=\int_0^\beta d\tau\int_0^\beta d\tau' c^\dagger(\tau)\mathbf{a}(\tau,\tau')c(\tau') + \int_0^\beta d\tau\sum_{j=0}^{N-1} Un_{j,\uparrow}(\tau)n_{j,\downarrow}(\tau), \tag{18}$$

with $\mathbf{a}$ the $2N\times 2N$ matrix mean-field function. To derive the semiclassical approximation we rewrite the interaction term as

$$Un_{j,\uparrow}(\tau)n_{j,\downarrow}(\tau)=\frac{U}{4}[N_j^2(\tau)-M_j^2(\tau)], \tag{19}$$

with $n_\uparrow n_\downarrow=\frac{1}{4}[(n_\uparrow+n_\downarrow)^2-(n_\uparrow-n_\downarrow)^2]=\frac{1}{4}(N^2-M^2)$. N is the number of particles and M is the magnetization on the site. We then make the usual continuous Hubbard-Stratonovich transformation to decouple the M terms via a site-dependent auxiliary field $\phi_j(\tau)$ which we assemble into an N-component vector $\vec{\phi}$. The semiclassical approximation is to retain only the zero-Matsubara-frequency term in the functional integral over ϕ. To this level of approximation the N term may be ignored because we work at half filling in a particle-hole-symmetric model. We may then integrate out the electrons and obtain

$$Z=\int d\vec{\phi}e^{S_{eff}[\mathbf{a},\phi]}, \tag{20}$$

where the effective action $S_{eff}=\beta V$ is defined by

$$V(\vec{\phi})=\frac{N}{U}|\vec{\phi}|^2-T\sum_{\omega_n,\sigma}\mathrm{Tr}\ln[-\mathbf{a}_\sigma(\omega_n)-\hat{\mathbf{1}}\tilde{\phi}\cdot\tilde{\sigma}], \tag{21}$$

with $\mathbf{1}$ the $2N\times 2N$ unit matrix.

The integral over ϕ is a simple classical integral which may be done without too much difficulty. However, at strong coupling and low temperatures V is characterized by several very deep minima with high barriers between them and it convenient to make a further simplification and approximate the integration over ϕ by the sum over the minima:

$$Z\approx\frac{1}{N_{min}}\sum_{j=1}^{N_{min}}e^{-\beta V(\vec{\phi}_j)}, \tag{22}$$

where N_{min} is the number of minima in potential $V(\vec{\phi})$. This approximation corresponds to approximating the spins as Ising variables.

The semiclassical approximation is reasonably good in the strong-coupling regime. It reproduces all of the qualitative features found in the QMC calculations and is reasonably quantitatively accurate. As an example, Fig. 4 shows the density of states calculated by analytical continuation of QMC and semiclassical data for the single-inpurity Hubbard model. One sees that the semiclassical method places the Hubbard bands very close to the correct positions. Similarly, Fig. 5 shows the on-site and first-neighbor spectral functions computed using the real-space (upper panel) and DCA

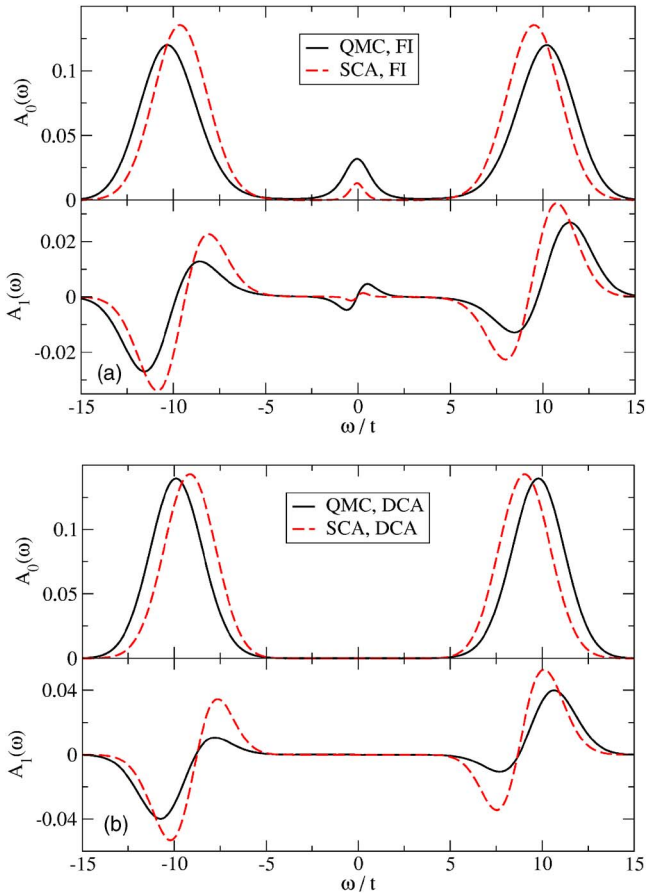

FIG. 5. (Color online) Two-site fictive-impurity (upper panel) and two-site DCA (lower panel) results for the spectral functions $A_0=-\frac{1}{\pi}\,\mathrm{Im}\,G_0$ and $A_1=-\frac{1}{\pi}\,\mathrm{Im}\,G_1$ computed by the QMC and SCA methods. $U/t=20$ and $T/t=0.5$, paramagnetic order.

(lower panel) two-site approximation to the square-lattice Hubbard model for the same parameters. Note that the unphysical feature in the density of states near $\omega=0$ (to be discussed in more detail below) evident in the real-space calculations but not in DCA is reproduced (or not reproduced) by the semiclassical approximation as appropriate, although the magnitude is not accurately determined

To summarize, the semiclassical and QMC methods yield very similar results for the parameters relevant to this study. The semiclassical method is orders of magnitude less computationally expensive. For example, performing one two-site cluster calculation at $U/t=20$ and $T/t=0.5$ required about 24 h on a 2.4 GHz Pentium computer, essentially because the partitioned phase space means that up to 10^7 configurations must be generated to sample the entire phase space adequately. By contrast the semiclassical calculation requires about 5 min on the same computer. Therefore most of the results presented below are obtained from SCA calculations.

III. NUMERICAL RESULTS

A. Overview

In this section we present numerical results obtained by the methods described in the previous sections and we compare these to high-temperature series results. We study four quantities: the local density of states

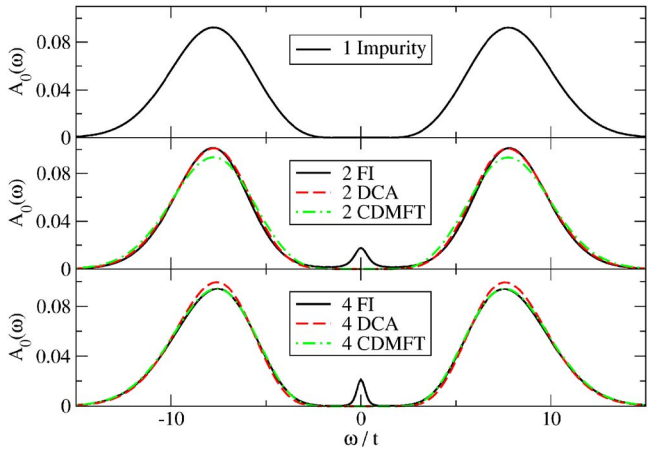

FIG. 6. (Color online) Spectral functions, obtained by the FI method, DCA, and CDMFT at $U/t=16$ and $T/t=0.3$, for one- (upper panel), two- (middle panel), and four- (lower panel) site clusters, using the SCA approximation with antiferromagnetism suppressed so model is in the paramgnetic phase.

$$N(\omega) = -\frac{1}{\pi}\int \frac{d^2p}{(2\pi)^2}\,\mathrm{Im}\,G(p,\omega), \tag{23}$$

the internal energy, given in the paramagnetic state by (the 2 is for the spin sum)

$$E = 2\int \frac{d\omega}{\pi}\int \frac{d^2p}{(2\pi)^2} f(\omega)\mathrm{Im}\left[\left(\varepsilon_p + \frac{1}{2}\Sigma(p,\omega)\right)G(p,\omega)\right], \tag{24}$$

the *impurity-model* nearest-neighbor (NN) spin-spin correlation function $\langle\sigma_1\sigma_2\rangle$, and the phase diagram.

B. Density of states

Figure 6 shows the single-particle density of states, calculated by maximum-entropy analytical continuation of our numerical solution of the dynamical mean-field equations, for the paramagnetic phase of the square-lattice Hubbard model with $U/t=16$ and $T/t=0.3$. (For the real-space approximation scheme this temperature is below the actual Néel temperature. In the data shown in Fig. 6 the magnetism has been suppressed to present results in the paramagnetic phase for all cases considered). The upper panel shows the spectral function computed from the single-site DMFT; the model is obviously in the Mott insulating phase, with well-separated upper and lower Hubbard bands. The middle panel shows the real-space, DCA, and CDMFT results for the density of states obtained from a two-site cluster. As in the single-impurity model, one observes the two Hubbard bands. The narrowing of the bands relative to the single-impurity case is a consequence of intersite magnetic correlations; indeed, even in the one-site model, in the fully ordered antiferromagnetic case the bands are substantially narrower than in the paramagnetic phase. One also sees that in the real-space (FI)

method a small band of midgap states exists. The lowest panel shows results obtained from four-site clusters. One sees clearly in the FI method that the area of the midgap states decreases as the cluster size increases and the frequency dependence changes. In a Mott insulator, the on-site self-energy diverges as $\omega \to 0$. The midgap states imply that in the FI cluster approximation Σ becomes small for some $\omega \approx 0$. These results suggest that convergence to the infinite-cluster-size limit is not uniform in frequency.

C. Internal energy

In this subsection we present results for the internal energy $E=\langle H \rangle$ computed from Eq. (24). We remove the Hartree shift $U/4$ and the chemical potential. We compare the calculated results to analytical large-U results, which have been obtained up to $\mathcal{O}(t^4/U^3)$.[25,26] To order t^2/U one has

$$E^{(2)} = -2\frac{t^2}{U}\tanh\left(\frac{U}{4T}\right) + \frac{t^2\left\{\frac{U}{2T}\tanh\left(\frac{U}{4T}\right) - 3\right\}}{2T\cosh^2\left(\frac{U}{4T}\right)}. \quad (25)$$

$E^{(2)}$ is shown as the light dotted line in Fig. 7. It includes terms from virtual excursions of an electron from one site to neighboring sites, but these average incoherently over the different relative spin orientations, and do not involve intersite correlations.

In this model at half filling, the nontrivial intersite physics is spin correlations and appears first at $\mathcal{O}(t^4/U^2T) \sim J^2/T$. To obtain results to this order we computed $E=\Omega - T\partial\Omega/\partial T$ numerically from the expressions for the thermodynamic potential Ω presented by Kubo.[26] The result is plotted as a heavy dashed line in each panel of Fig. 7.

Internal energy results as a function of temperature at $U/t=16$ are shown in Fig. 7 for the real-space (upper panel), DCA (middle panel), and CDMFT (lower panel) schemes, along with analytical results. For the dynamical mean-field methods, we show results in both the paramagnetic state and antiferromagnetic state. The calculated Néel temperature is visible as the point of discontinuity in the $E(T)$ curves; for $T<T_N$, we show both the antiferromagnetic state energy (lower curve) and the energy of the paramagnetic state (obtained by artificially suppressing the Néel state). We note that in order to obtain accurate energies the high-frequency behavior of the Green functions must be carefully controlled.

All of the curves display three temperature regimes: a very-high-T regime (for the parameters considered here, beginning at $T/t>0.75$) where the energy increases with increasing T, an intermediate-T regime (here $\approx 0.5 < T/t < 0.75$) where the energy is approximately T independent, and a low-T regime in which the energy exhibits a strong T dependence. The increase of E with T in the high-T regime arises from real thermal excitations over the Mott-Hubbard gap [cf. the second term in Eq. (25)]. The more rapid upturn of the DMFT results relative to the series expansion is an artifact of the SCA, which overestimates the effect of thermal flucuations on the gap. This regime will not be discussed further here.

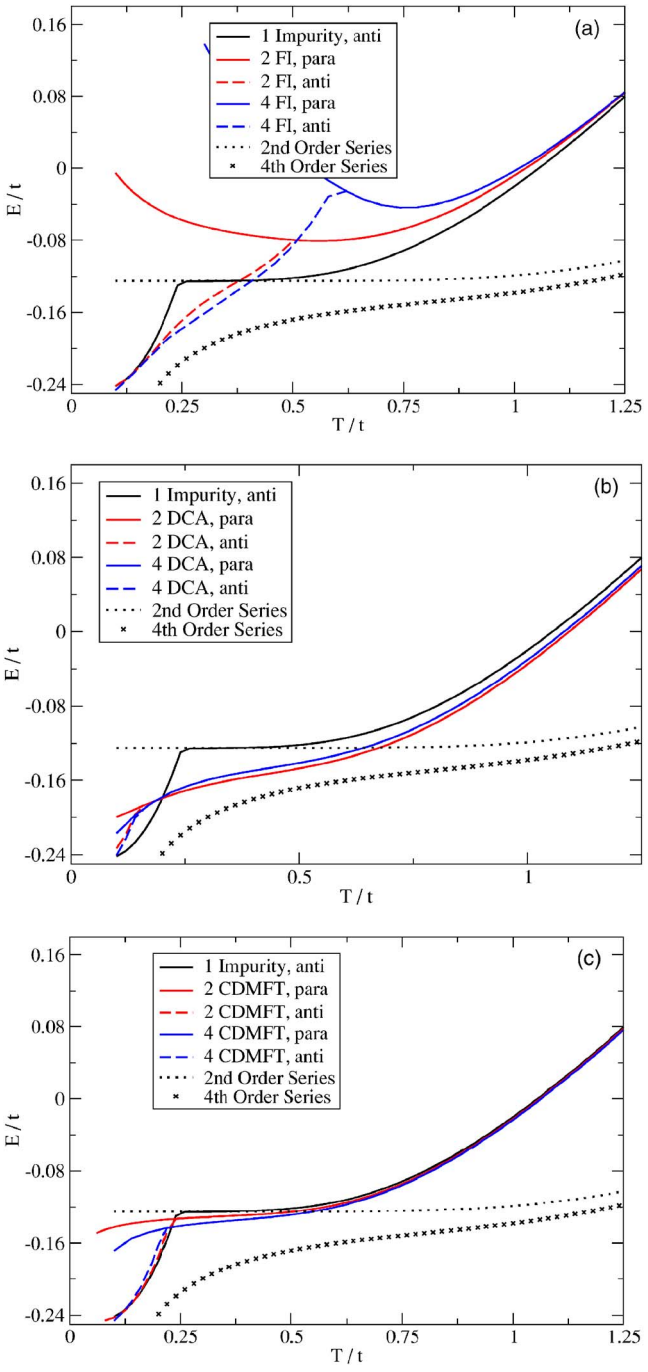

FIG. 7. (Color online) Internal energy E/t as a function of temperature obtained by FI method (upper panel), DCA (middle panel), and CDMFT (lower panel) at $U/t=16$ using the SCA and compared to analytical results. Thick solid curves are for single impurity, solid (solid with squares) curves for a two-site (four-site) cluster in an antiferromagnetic state, and dashed (dashed with squares) curves for a two-site (four-site) cluster in paramagnetic state, and stars and crosses are obtained as described in the text from the large U expansion, to the order in U indicated. The rapid rise with temperature of the DMFT results for temperatures $T>t$ is an artifact of the implementation of the semiclassical approximation based on Eq. (22) used here, which overestimates the contribution of excitations across the upper Hubbard band.

In the intermediate-T regime, the excitations into the upper Hubbard band are quenched and intersite spin correlations are slowly developing. The single-site DMFT neglects intersite correlations entirely in the paramagnetic phase; thus, in this regime the single-site DMFT result is essentially independent of temperature and is seen to be very close to the second-order series result $t/U=0.0625$; we would expect corrections to be of relative order $1/U^2 \sim 10^{-2}$, essentially invisible. The effect of intersite correlations is visible below the Néel temperature.

Both 2FI and 4FI methods produce energies which lie above the single-site DMFT curves and which increase at low T. We conclude that in these methods the intersite spin correlations are wrongly treated, leading to an $\mathcal{O}(J^2/T)$ contribution to the energy with the wrong sign. The physical origin of the error is the midgap states which shift weight of order t^4/U^4 in Im G from the vicinity of the lower Hubbard band up to the chemical potential, thereby raising the energy.

The CDMFT and DCA methods produce energies which lie below the single-site curve, indicating that they provide a qualitatively correct treatment of the intersite spin correlations. The quantitative accuracy may be judged from the separation between the DMFT calculations and the series results. The agreement is not impressive. The CDMFT intersite energy is far too small, while in the DCA method the four-site cluster produces an energy in worse agreement with the correct answer than does the two-site cluster.

Finally, we note that in the four-site methods, if the Néel ordering is suppressed, an apparent first-order transition (most probably to a dimerized spin state) occurs.

D. Néel temperature

The Néel transition temperature T_N was identified with the temperature corresponding to the kink in the antiferromagnetic $E(T)$ curve. We have verified the values by writing an independent code to obtain the temperature dependence of the staggered magnetization. We note that our methods are mean-field methods. In the two-dimensional models studied here spatial fluctuations drive T_N logarithmically to zero. We also note that the SCA+Ising-spin approximation used here is not able to capture dimer states. Our computed Néel temperature is therefore best interpreted as a scale below which the spin-spin correlations become appreciable. The computed mean-field phase diagram is shown in Fig. 8. In the small-U limit all the methods agree reasonably well with each other and with the simple analytical results. This finding is in agreement with a detailed study of the size dependence of the Néel temperature at small U.[27] However, at large U substantial variation exists. The FI method grossly overestimates T_N. We believe that the overestimate occurs because the ordering eliminates the midgap states, thereby substantially lowering the energy, (cf. Fig. 7). The unphysical nature of the FI results means that computations of the four-site FI method are not worth performing and are not presented here.

E. Impurity-model spin correlations

We finally consider the spin correlations in the impurity model. (Note that the "fictive" nature of the impurity model means that it is not to be thought of as a physical subcluster of the lattice, so the relation of the impurity-model spin correlations to the actual spin correlations in the lattice is not entirely straightforward.) In Fig. 9 we show the comparison of the NN spin-spin correlation to the two- and four-site CDMFT (lower panel), DCA (middle panel), and FI method (upper panel) results as a function of temperature. Also included is the leading term $\langle \sigma_1 \sigma_2 \rangle = -t^2/(TU)$ in the appropriate high-temperature-series expansion. We see that the various methods obtain results which have the correct temperature dependence, but with magnitudes somewhat at variance with the exact results. We observe that the underestimate of the intersite contribution to the energy is not reflected in an underestimate of the cluster spin-spin correlations, suggesting that the deficiencies of the methods have to do with interactions which extend outside the cluster considered. We also note that for the sizes available to us, increasing cluster size does not lead to improved agreement.

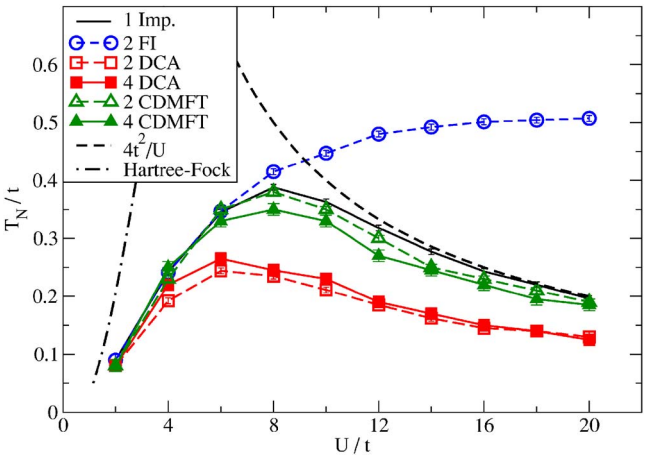

FIG. 8. (Color online) Néel temperature T_N/t vs on-site interaction U/t obtained by the SCA. Solid curves are fits of the data.

IV. APPROXIMATE ANALYTICAL TREATMENT

A. General formulation

In this section we present approximate analytical calculations which provide some insight into the numerical results. The calculations are based on an approximation to the semiclassical method of Ref. 23. This first subsection gives some general considerations. The next subsection presents the relevant aspects of the approximate solution of the impurity model (which is the same for all methods). Subsequent sections combine these formulas with appropriate self-consistency conditions to obtain results for the single-site model and the two- and four-site DCA, CDMFT, and FI approaches.

In developing the analytical approximations it is useful to alternate between two basis choices for the impurity model: first, a real-space basis with on-site a_0 and intersite $a_{j\neq 0}$ mean-field parameters. The key simplification of the large-U half-filled limit is easily seen in this basis: the magnitude of the intersite terms $a_{i\neq 0}$ is much less than $|a_0^2 - \phi^2|$. Assuming no spatial symmetry breaking (so $|\phi|$ is the same on all sites)

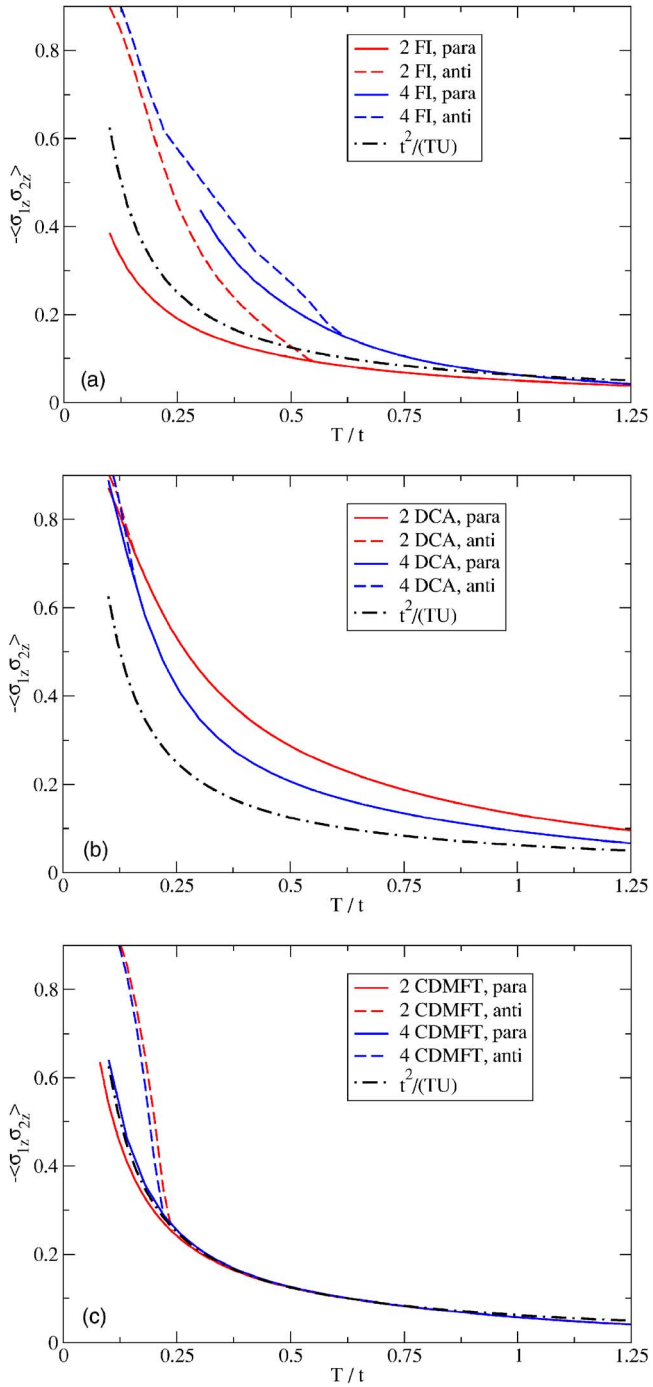

FIG. 9. (Color online) Nearest-neighbor spin-spin correlation as a function of temperature obtained by the FI method (upper panel), DCA (middle panel), and CDMFT (lower panel) at $U/t=16$ using the SCA and the Ising spin approximation (see also Sec. IV). Also shown is the high-temperature series result for the Ising approximation to the square-lattice Heisenberg model $\langle\sigma_{1z}\sigma_{2z}\rangle=-t^2/(TU)$, which is the result to which it is appropriate to compare the numerical calculations performed using Eq. (22).

and expanding to second order in the parameter $a_{i\neq 0}^2/(a_0^2-\phi^2)$ leads to an expression involving the mean-field parameters and the intersite spin correlations, which may be treated analytically.

For solving the self-consistency condition it is more convenient to consider the impurity-model eigenbasis. An N-site impurity model involves an $N\times N$ matrix mean field function $\mathbf{a}$, Green function $\mathbf{G}$, and self-energy $\mathbf{\Sigma}$ related by $\mathbf{\Sigma}=\mathbf{a}-\mathbf{G}^{-1}$. We restrict our attention to the paramagnetic phase so $\mathbf{a}$, $\mathbf{G}$, and $\mathbf{\Sigma}$ are proportional to the unit matrix in spin space. For the models of interest the orbital-space matrices may be simultaneously diagonalized, so that for the N eigenmodes λ we have

$$G_\lambda=(a_\lambda-\Sigma_\lambda)^{-1}. \tag{26}$$

The DMFT self-consistency equation is obtained by relating the lattice and impurity-model Green functions. Different schemes involve different methods for relating the impurity-model Green function and self-energy to the lattice Green function and self-energy. In the impurity-model eigenbasis we have

$$a_\lambda-\Sigma_\lambda=\left(\left[\int(dk)\frac{1}{i\omega-\varepsilon_k-\Sigma(k,\omega)}\right]_\lambda\right)^{-1}. \tag{27}$$

Here the notation $[\int(dk)]_\lambda$ denotes the details required for the particular DMFT scheme. We may then expand the right-hand side, noting that in a Mott insulator $|i\omega-\Sigma|\gg|\varepsilon_k|$ and that $\Sigma(k,\omega)=\Sigma_\lambda+s_k^{(1)}=\frac{U^2}{4i\omega}+s_k^{(2)}$ with $s_k^{(1,2)}$ small. This formulation enables one to solve for the mean-field parameters without explicitly computing the Green functions or the subleading contributions to the self-energy.

In the rest of this section we present the details of the large-U analysis. We first give the analytical solution of the general impurity model, then present the connection to the lattice, and finally give results for physical quantities.

B. Impurity-model and self-consistency condition: Large-U limit

An N-site impurity model is specified by a set of $P+1$ $N\times N$ matrices $\mathbf{M}_i$. The impurity-model action S_{imp} is

$$S_{imp}=\sum_{j=0}^{P}a_j\mathbf{M}_j+H_{int}. \tag{28}$$

For all models, $\mathbf{M}_0$ is the $N\times N$ unit matrix $\mathbf{1}$. For the two-site model, $\mathbf{M_1}=\tau_x$ and the eigenvectors are correspondingly the even and odd combinations

$$a_e=\frac{1}{\sqrt{2}}(a_0+a_1), \tag{29}$$

$$a_o=\frac{1}{\sqrt{2}}(a_0-a_1). \tag{30}$$

For the four-site model, $P=2$ with

$$\mathbf{M}_1=\frac{1}{\sqrt{2}}\begin{pmatrix}0&1&0&1\\1&0&1&0\\0&1&0&1\\1&0&1&0\end{pmatrix}, \tag{31}$$

$$\mathbf{M}_2 = \begin{pmatrix} 0 & 0 & 1 & 0 \\ 0 & 0 & 0 & 1 \\ 1 & 0 & 0 & 0 \\ 0 & 1 & 0 & 0 \end{pmatrix}. \tag{32}$$

The eigenvectors are

$$|S\rangle = \frac{1}{2}\begin{pmatrix} 1 \\ 1 \\ 1 \\ 1 \end{pmatrix}, \quad |X\rangle = \frac{1}{\sqrt{2}}\begin{pmatrix} 1 \\ 0 \\ -1 \\ 0 \end{pmatrix},$$

$$|Y\rangle = \frac{1}{\sqrt{2}}\begin{pmatrix} 0 \\ 1 \\ 0 \\ -1 \end{pmatrix}, \quad |D\rangle = \frac{1}{2}\begin{pmatrix} 1 \\ -1 \\ 1 \\ -1 \end{pmatrix},$$

so

$$a_S = a_0 + \sqrt{2}a_1 + a_2, \tag{33}$$

$$a_X = a_0 - a_2, \tag{34}$$

$$a_Y = a_0 - a_2, \tag{35}$$

$$a_D = a_0 - \sqrt{2}a_1 + a_2. \tag{36}$$

To solve the impurity model we proceed from Eq. (20) in the large-U limit. We treat the integral over the magnitude of the auxiliary field by the steepest-descent approximation, so that in the large-U limit $|\phi| \approx U/2$ is the same on each site but the direction $\hat{\Omega}_j$ may vary. Corrections to the steepest-descent approximation (Gaussian fluctuations about the saddle point) give subleading corrections to the results we will present. The partition function is then

$$Z \approx \int (d\hat{\Omega}_j) e^{-\beta V_{eff}(\{\hat{\Omega}_j\})}, \tag{37}$$

with the $|\phi|$ fixed by $\frac{\partial V}{\partial \phi_j} = 0$.

We consider temperatures low enough that thermal excitation into the upper Hubbard band may be neglected [mathematically this means we replace $T\Sigma_{\omega_n}$ by $\int d\omega/(2\pi)$ in all expressions, with one exception discussed below].

The Hubbard-Stratonovich transformation followed by integration over the fermion fields leads, in the semiclassical approximation, to

$$S_{imp} = \mathrm{Tr}\ \ln\left[\sum_{j=0,P} a_j \mathbf{M}_j - \phi \mathbf{D}\right] - \frac{N\phi^2}{U}, \tag{38}$$

with $\mathbf{D}$ a diagonal matrix with entries $\phi\vec{\Omega}_i \cdot \vec{\sigma}$. At large U and half filling we have $|a_0^2 - \phi^2| \gg |a_{j\neq 0}|^2$. Expanding to second order gives

$$S_{imp} = -\frac{N\phi^2}{U} + N\mathrm{Tr}\ \ln[a_0^2 - \phi^2] - \sum_{i,j\neq 0} \frac{a_i a_j}{2(a_0^2 - \phi^2)^2} \mathrm{Tr}[\mathbf{M}_i(a_0\mathbf{1} + \mathbf{D})\mathbf{M}_j(a_0\mathbf{1} + \mathbf{D})]. \tag{39}$$

Taking the trace explicitly yields, for two- and four-site models,

$$S_{imp}^2 = -\frac{2\phi^2}{U} + 2\mathrm{Tr}\ \ln[a_0^2 - \phi^2] - \frac{2a_1^2(a_0^2 + \phi^2\hat{\Omega}_1 \cdot \hat{\Omega}_2)}{(a_0^2 - \phi^2)^2}, \tag{40}$$

$$S_{imp}^4 = -\frac{4\phi^2}{U} + 4\mathrm{Tr}\ \ln[a_0^2 - \phi^2] - \frac{a_1^2\{4a_0^2 + \phi^2(\hat{\Omega}_1 \cdot \hat{\Omega}_2 + \hat{\Omega}_2 \cdot \hat{\Omega}_3 + \hat{\Omega}_3 \cdot \hat{\Omega}_4 + \hat{\Omega}_4 \cdot \hat{\Omega}_1)\}}{(a_0^2 - \phi^2)^2} - \frac{a_2^2\{2a_0^2 + 2\phi^2(\hat{\Omega}_1 \cdot \hat{\Omega}_3 + \hat{\Omega}_2 \cdot \hat{\Omega}_4)\}}{(a_0^2 - \phi^2)^2}. \tag{41}$$

We shall see that for the Hubbard model with nearest-neighbor hopping, $a_2 = 0$ to the order to which we work. In this case, for both two- and four-site models, the mean-field equation fixing ϕ is

$$\frac{1}{U} = -T\sum_n \left[\frac{1}{a_0^2 - \phi^2} + \frac{a_1^2[2a_0^2 + S(a_0^2 + \phi^2)]}{(a_0^2 - \phi^2)^3}\right], \tag{42}$$

with S the nearest-neighbor spin correlation given for $N = 2, 4$ by

$$S = \langle \hat{\Omega}_1 \cdot \hat{\Omega}_2 \rangle \approx -\frac{4}{3N}\sum_n \frac{a_1^2\phi^2}{(a_0^2 - \phi^2)^2}, \tag{43}$$

where the second approximate equality comes from expanding Z to leading order in $a_1^2/(a_0^2 - \phi^2)$ and applies for T sufficiently greater than $J = t^2/U$. Note that Eq. (43) is written for Heisenberg spins; the semiclassical numerical method used here amounts to an Ising approximation in which the prefactor becomes $4/N$.

For comparison to the numerics we note that in the Ising approximation used in the numerical calculations the factor of 3 in the denominator of the right-hand side of Eq. (43) is absent.

The impurity-model Green functions are $\mathbf{G}_j^{imp} = g_j \mathbf{M}_j$ with $g_j = \delta \ln Z/(2N\delta a_j)$. In both two- and four-site models we find (assuming $a_2 = 0$)

$$g_0 = \frac{a_0}{a_0^2 - \phi^2}\left(1 + \frac{a_1^2[a_0^2 + \phi^2(1 + 2S)]}{(a_0^2 - \phi^2)^2}\right), \tag{44}$$

$$g_1 = \frac{-a_1(a_0^2 + \phi^2 S)}{(a_0^2 - \phi^2)^2}. \tag{45}$$

General expressions for the self-energy are cumbersome. By combining g_0 and g_1 into the appropriate impurity-model eigencombinations we find that

$$\Sigma_\lambda = \frac{\phi^2}{a_0}\left\{1 + \mathcal{O}\left(\frac{tS}{U}\right)\right\}. \tag{46}$$

In the low-frequency limit $|\omega| \ll \phi$ we have, for the two-site model,

$$\Sigma_e = \frac{\phi^2}{a_0 + a_1 S}, \tag{47}$$

$$\Sigma_o = \frac{\phi^2}{a_0 - a_1 S}, \tag{48}$$

while for the four-site model,

$$\Sigma_S = \frac{\phi^2}{a_0 + a_1 S}, \tag{49}$$

$$\Sigma_X = \frac{\phi^2}{a_0}, \tag{50}$$

$$\Sigma_Y = \frac{\phi^2}{a_0}, \tag{51}$$

$$\Sigma_D = \frac{\phi^2}{a_0 - a_1 S}. \tag{52}$$

For the impurity models in the insulating regime, we will find that $a_0 \sim \omega$ while $a_1 \sim t$. Thus the low-frequency behavior of the impurity-model self-energies is well approximated by the simple pole

$$\Sigma_\lambda(z) \approx \frac{\mathcal{R}_\lambda}{z - \Omega_\lambda}. \tag{53}$$

In the single-site dynamical mean-field approximation, $\Omega_\lambda = 0$, but in general Ω_λ is of order t with a prefactor which depends on the intersite spin correlations and becomes very small at $T > t^2/U = J$.

Differences between dynamical mean-field schemes arise from different ways of combining the impurity-model self-energies into an approximation to the lattice self-energy. In the DCA and CDMFT approaches, the impurity-model self-energy translates essentially directly into a lattice self-energy, so that the pole structure is preserved. In the FI approach, the situation is different. For example, in the two-site model one has, at low frequency,

$$\Sigma_{FI}(\omega) \approx \phi^2\left(\frac{1 + 2d\gamma_k}{\omega - \Omega_e} + \frac{1 - 2d\gamma_k}{\omega - \Omega_o}\right), \tag{54}$$

with $\Omega_e \neq \Omega_o$. Equation (54) implies that at a general k the approximate self-energy has two poles with a zero crossing between them. This incorrect analytical structure leads to the midgap states found numerically.

C. Single-site approximation

In the single-site problem, the on-site terms are the only ones present, so we set $a_1 = S = 0$ in the formulas of the previous section. The impurity-model Green function is

$$G_{imp} = \frac{a_0}{a_0^2 - \phi^2}, \tag{55}$$

so that

$$\Sigma = \frac{\phi^2}{a_0}. \tag{56}$$

The self-consistency equation is $(dk) = d^d k/(2\pi)^d$:

$$a_0 - \Sigma = \left[\int (dk)\frac{1}{i\omega - \Sigma - \varepsilon_k}\right]^{-1}. \tag{57}$$

Now in a Mott insulator we expect $|i\omega - \Sigma| \gg |\varepsilon_k|$. Thus we rewrite Eq. (57) as

$$\begin{aligned} a_0 - \Sigma &= (i\omega - \Sigma)\left[\int (dk)\frac{1}{1 - \dfrac{\varepsilon_k}{i\omega - \Sigma}}\right]^{-1} \\ &= (i\omega - \Sigma)\left\{1 + \frac{K_d}{(i\omega - \Sigma)^2}\right\}, \end{aligned} \tag{58}$$

where

$$K_d = \int (dk)\varepsilon_k^2 = 2dt^2. \tag{59}$$

Thus

$$a_0 = i\omega\left(1 + \frac{K_d}{\omega^2 + \phi^2}\right), \tag{60}$$

$$\Sigma = \frac{\phi^2}{i\omega}\left(1 - \frac{K_d}{\omega^2 + \phi^2}\right), \tag{61}$$

while substitution into Eqs. (42) and (24) and expansion and replacement of the frequency sums by integrals gives

$$\phi = \frac{U}{2} - \frac{K_d}{2U}, \tag{62}$$

$$E = -\frac{U}{8} - \frac{K_d}{4U} = -\frac{U}{8} - \frac{dt^2}{2U}. \tag{63}$$

We observe that to this order in the t/U expansion the single-site DMFT is in agreement with the exact result, Eq. (25).

D. DCA

In the DCA one covers the Brillouin zone with N tiles, λ, which correspond to the eigenvectors of the impurity model. The self-consistency equations are

$$a_\lambda - \Sigma_\lambda = \left[\int_\lambda (dk) \frac{1}{i\omega - \varepsilon_k - \Sigma_\lambda} \right]^{-1}, \tag{64}$$

where $\int_\lambda (dk)$ denotes an integral over tile λ of the Brillouin zone, normalized so $\int_\lambda (dk)=1$. An analysis identical to that leading to Eq. (57) gives, up to corrections of order t^3/U^2,

$$a_\lambda = i\omega - I_\lambda - \frac{K_\lambda - I_\lambda^2}{i\omega - \frac{\phi^2}{i\omega}}, \tag{65}$$

with

$$I_\lambda = \int_\lambda (dk) \varepsilon_k, \tag{66}$$

$$K_\lambda = \int_\lambda (dk) \varepsilon_k^2. \tag{67}$$

Note that in the limit spatial dimensionality $d \to \infty$ $K \sim d$ whereas $\Sigma_\lambda I_\lambda \sim 1$ so that in this limit the model reduces to single-site dynamical mean-field theory.

In the two-site DCA the two eigenstates are even (e) and odd (o) and we find (in $d=2$)

$$I_e = -I_o = -I^{(2)} = \frac{16t}{\pi^2} \approx -1.62t, \tag{68}$$

$$K_e = K_o = K^{(2)} = 4t^2, \tag{69}$$

implying

$$a_0 = i\omega \left\{ 1 + \frac{K^{(2)} - (I^{(2)})^2}{\omega^2 + \phi^2} \right\}, \tag{70}$$

$$a_1 = -I_e = \frac{16t}{\pi^2}. \tag{71}$$

In the four-site DCA we have

$$I_S = -I_D = -\frac{8t}{\pi} \approx -2.55t, \tag{72}$$

$$I_X = I_Y = 0, \tag{73}$$

$$K_S = K_D = 4t^2 + \frac{32t^2}{\pi^2} \approx 7.24t^2, \tag{74}$$

$$K_X = K_Y = 4t^2 - \frac{32t^2}{\pi^2} \approx 0.76t^2. \tag{75}$$

Let us define

$$I^{(4)} = -\frac{1}{2\sqrt{2}}(I_S - I_D) = \frac{4\sqrt{2}t}{\pi} \approx 1.80t, \tag{76}$$

$$K^{(4)} = \frac{1}{4} \sum_{\lambda = S,X,Y,D} K_\lambda = 4t^2. \tag{77}$$

Then

$$a_0 = i\omega \left\{ 1 + \frac{K^{(4)} - (I^{(4)})^2}{\omega^2 + \phi^2} \right\}, \tag{78}$$

$$a_1 = I^{(4)}. \tag{79}$$

Thus for the $N=2,4$ site models the Ising version of Eq. (43) implies

$$S = -\frac{I^2}{N\phi T} \approx -\frac{2I^2}{NTU}, \tag{80}$$

with I given by either $I^{(2)}$ or $I^{(4)}$ as appropriate. From Eq. (42) we have

$$\begin{aligned} \frac{\phi}{U} &= \int_{-\infty}^{\infty} \frac{d\omega}{2\pi} \left[\frac{\phi}{\omega^2 \left(1 + \frac{K - I^2}{\omega^2 + \phi^2} \right)^2 + \phi^2} \right. \\ &\quad \left. + \frac{I^2 \{ -2\omega^2 + S(-\omega^2 + \phi^2) \}}{(\omega^2 + \phi^2)^3} \right] \\ &= \int_{-\infty}^{\infty} \frac{d\omega}{2\pi} \left[\frac{\phi}{\omega^2 + \phi^2} \left\{ 1 - 2\frac{K - I^2}{(\omega^2 + \phi^2)^2} \right\} \right. \\ &\quad \left. + \frac{I^2 \phi \{ -2\omega^2 + S(-\omega^2 + \phi^2) \}}{(\omega^2 + \phi^2)^3} \right] \\ &= \int_{-\infty}^{\infty} \frac{d\omega}{2\pi} \left[\frac{\phi}{\omega^2 + \phi^2} \left\{ 1 - 2\frac{K\omega^2}{(\omega^2 + \phi^2)^2} \right\} \right. \\ &\quad \left. + \frac{I^2 S \phi (-\omega^2 + \phi^2)}{(\omega^2 + \phi^2)^3} \right] \\ &= \frac{1}{2} - \frac{K}{2U^2} + \frac{I^2 S}{2U}, \end{aligned} \tag{81}$$

with K given by $K^{(2,4)}$ as appropriate.

Finally, we consider the energy. Within the DCA we have

$$\begin{aligned} E_{DCA} &= 2T \sum_{n,\lambda} \int_{T_\lambda} (dp) \frac{\varepsilon_p + \frac{1}{2}\Sigma_\lambda(\omega_n)}{i\omega_n - \varepsilon_p - \Sigma_\lambda(\omega_n)} \\ &= \frac{2T}{N} \sum_{n,\lambda} \left[-1 + \left(i\omega_n - \frac{1}{2}\Sigma_\lambda \right) G_\lambda(i\omega_n) \right]. \end{aligned} \tag{82}$$

We now rearrange Eq. (82) into a form more convenient for the strong-coupling expansion. We write $G_\lambda = (a_\lambda - \Sigma_\lambda)^{-1}$ and by adding and subtracting obtain

$$E = T \sum_n \left[(i\omega_n G_0 - 1) + \frac{1}{N} \sum_\lambda (i\omega_n - a_\lambda) G_\lambda(i\omega_n) \right]. \tag{83}$$

Finally, we note that because the same change of basis diagonalizes $\mathbf{G}$ and $\mathbf{a}$ and $\mathbf{G} = \sum_{a=0}^{N-1} G_n \mathbf{M}_n$ and similarly for $\mathbf{a}$ with $\mathrm{Tr}\,[\mathbf{M}_i \mathbf{M}_j] = N\delta_{ij}$, we have

$$E = T\sum_n \left[(a_0 G_0 - 1) + 2(i\omega_n - a_0)G_0 - \sum_{b=1}^{N-1} a_b G_b \right]. \tag{84}$$

Here each of the three terms is convergent at large ω and the second and third are explicitly of order t^2/U.

We consider the three terms in turn. The first term is, explicitly,

$$\begin{aligned} E^{(1)} &= T\sum_n (a_0 G_0 - 1) \\ &= T\sum_n \frac{a_0^2}{a_0^2 - \phi^2}\left[1 + \frac{a_1^2\{a_0^2 + \phi^2(1+2S)\}}{(a_0^2 - \phi^2)^2} \right] - 1 \\ &= T\sum_n \left[\frac{\phi^2}{a_0^2 - \phi^2} + \frac{a_1^2 a_0^2\{a_0^2 + \phi^2(1+2S)\}}{(a_0^2 - \phi^2)^3} \right] \\ &= -\frac{U}{4} + \frac{K - I^2}{2U}. \end{aligned} \tag{85}$$

Similarly, use of Eq. (70) gives

$$E^{(2)} = T\sum_n 2(i\omega_n - a_0)G_0 = T\sum_n \frac{-2\omega^2(K - I^2)}{(a_0^2 - \phi^2)^2} = -\frac{K - I^2}{U}, \tag{86}$$

while

$$E^{(3)} = -T\sum_n a_1 G_1 = -T\sum_n \frac{a_1^2(a_0^2 + \phi^2 S)}{(a_0^2 - \phi^2)^2} = -\frac{I^2}{2U}(1 - S). \tag{87}$$

Thus the total energy for the $N=2,4$ site DCA approximation is

$$E_{DCA}^N = -\frac{U}{4} - \frac{K}{2U} + \frac{(I^{(N)})^2 S}{2U} = -\frac{U}{4} - \frac{K}{2U} - \frac{(I^{(N)})^4}{NU^2 T}, \tag{88}$$

so that

$$E^{2\text{-}DCA} \approx -3.45\frac{t^4}{U^2 T}, \tag{89}$$

$$E^{4\text{-}DCA} \approx -2.62\frac{t^4}{U^2 T}. \tag{90}$$

We see that both two- and four-site DCA approximations lead to an expression for the energy which reduces to the single-site expression if the spin correlation $S=0$. The differences between the two- and four-site approximations have a small contribution from the difference in the factors I but this is overcompensated by the factor of N in Eq. (43). Numerically the coefficient of the $1/T$ term is seen to be larger for the two-site DCA than for the four-site DCA, so that (in agreement with the numerical results) the four-site DCA is seen to have a slightly worse intersite energy than the two-site DCA.

E. CDMFT

The CDMFT approximation may be treated in a manner very similar to the DCA. The lattice Green function is a matrix in the space of the cluster states, so the self-consistency equation is

$$\mathbf{G}_{imp} = \int' (dk)[i\omega - \Sigma - \mathbf{E}(k)]^{-1}, \tag{91}$$

where the prime denotes an integral over the reduced Brillouin zone appropriate to the real-space tiling and the dispersion matrix E was given above in Eqs. (10) and (12). Expanding and noting that $|i\omega\mathbf{1} - \mathbf{\Sigma}| \gg \mathbf{E}(p)$ and that $\mathbf{\Sigma}$ is diagonal to leading order in t/U we find

$$\mathbf{G}_{imp} = (i\omega - \Sigma)^{-1}[\mathbf{1} + \mathbf{I}(i\omega - \Sigma)^{-1} + \mathbf{K}(i\omega - \Sigma)^{-2}], \tag{92}$$

with

$$\mathbf{I} = \int' (dk)\mathbf{E}(k), \tag{93}$$

$$\mathbf{K} = \int' (dk)\mathbf{E}(k)^2, \tag{94}$$

Thus, inverting once more and using again that $\mathbf{\Sigma}$ is approximately diagonal we obtain

$$\mathbf{a} = i\omega\mathbf{1} - \mathbf{I} - \frac{\mathbf{K} - \mathbf{I}^2}{i\omega - \dfrac{\phi^2}{i\omega}}. \tag{95}$$

In the two-site CDMFT we have

$$\mathbf{I} = -t\begin{pmatrix} 0 & 1 \\ 1 & 0 \end{pmatrix}, \tag{96}$$

$$\mathbf{K} = -4t^2\begin{pmatrix} 1 & 0 \\ 0 & 1 \end{pmatrix}, \tag{97}$$

while in the four-site CMDFT we have

$$\mathbf{I} = -\sqrt{2}t\mathbf{M}_1 \approx -1.4t\mathbf{M}_1, \tag{98}$$

$$\mathbf{K} = -4t^2\left(\mathbf{M}_0 + \frac{1}{2}\mathbf{M}_2\right). \tag{99}$$

The solution of the self-consistency equations and the analysis of the energy go through as before; the only difference is in the values of the intersite parameters a_1. We find

$$I^{2\text{-}CDMFT} = -t, \tag{100}$$

$$I^{4\text{-}CDMFT} = -\sqrt{2}t, \tag{101}$$

so the intersite term in the energy is

$$\delta E^{2\text{-}CDMFT} \approx -0.5\frac{t^4}{U^2 T}, \tag{102}$$

$$\delta E^{4\text{-}CDMFT} \approx -\frac{t^4}{U^2 T}. \tag{103}$$

Thus the CMDFT method underestimates the intersite correlations by a larger factor than the DCA but moves in the correct direction with cluster size.

F. FI model

The analysis of the FI equations is not quite as straightforward as the analysis of the DCA and CDMFT equations. We specialize at the outset to the two-site problem, which reveals the essential difficulties. In this case, the lattice self-energy is (for the nearest-neighbor hopping model studied here)

$$\Sigma(k,\omega) = \frac{1+2d\gamma_k}{2}\Sigma_e + \frac{1-2d\gamma_k}{2}\Sigma_o \tag{104}$$

and the self-consistency equations are (for general d)

$$G_{e,o}^{-1} = \left[\int (dk)\frac{1\pm\gamma_k}{i\omega - \Sigma(k,\omega) - \varepsilon_k}\right]^{-1}. \tag{105}$$

Unlike the previously considered cases, the self-energy has a momentum dependence which interacts with the momentum dependence arising from the dispersion. Because Σ_e and Σ_o have poles at different energies [cf. Eqs. (47) and (48)], $\Sigma(k,\omega)$ generically has two poles (with k-dependent strengths) and (except at special k points) a zero crossing between them. This structure is physically incorrect (the self-energy should have only one pole at a given k) and the concomitant zero crossing produces the midgap states.

To analyze the equation, say, for G_e we write

$$\Sigma(k,\omega) = \Sigma_e(\omega) + \frac{\Sigma_o - \Sigma_e}{2}(1-2d\gamma_k), \tag{106}$$

assume the second term is small compared to the first, and proceed as before. We obtain (in spatial dimensionality d)

$$a_{e,o} = i\omega \mp t - \frac{K_d\left(1-\frac{\Sigma_1}{t}\right)^2}{\left(i\omega - \frac{\phi^2}{i\omega}\right)}\left[1-\frac{1}{2d}\right]. \tag{107}$$

Thus

$$a_1 = t, \tag{108}$$

and (again for the hypercubic lattice with nearest-neighbor hopping and keeping only terms up to order t^2/U^2)

$$a_0 = i\omega - \frac{2dt^2\left(1+\frac{\phi^2 S}{a_0^2}\right)^2}{i\omega - \frac{\phi^2}{a_0}}\left[1-\frac{1}{2d}\right]. \tag{109}$$

In the derivation of the single-site DMFT equations the $d\to\infty$ limit is taken with dt^2 held constant. In this limit, $S\sim t^2/(TU)\sim 1/d$ vanishes and the equations revert to the usual single-site DMFT form.

Equation (109) is valid for $T>\sqrt{Jt}$, but the solution changes character for $\omega<\sqrt{t^2U/T}$. At high frequencies we may solve iteratively, obtaining

$$a_0 \approx i\omega\left\{1+2dt^2\left(1-\frac{1}{2d}\right)\frac{\left(1-\frac{\phi^2 S}{\omega^2}\right)^2}{\omega^2+\phi^2}\right\}. \tag{110}$$

Thus, if S is sufficiently small, we find $a_0\sim\omega$ and $a_1\sim t$. At lower frequencies, the structure of the equation becomes more complicated, because of the presence of $\Sigma_1\sim 1/a_0^2$ on the right-hand side of the equation. This behavior arises because of the inappropriate combination of poles and produces the midgap states discussed above.

V. SUMMARY AND DISCUSSION

In this paper we have examined several multisite extensions of the dynamical mean-field method in the strong-coupling limit, which has not been the subject of previous systematic study. We have computed a variety of physical quantities and compared these to available and newly computed analytical results. We were able to isolate the contributions which arise from nontrivial intersite (in this case, spin-spin) correlations. We found that an incorrect treatment of these in a real-space (FI) scheme produces unphysical midgap states in the Mott insulating phase and thus wrongly estimates the internal energy, Néel temperature, and spin correlations. The DCA and CDMFT schemes did not lead to midgap states and produced results which are qualitatively correct. However, substantial quantitative differences exist between the CDMFT and DCA results and the exact answers.

From a mathematical point of view the central difficulty with the FI approach is the pole structure of the self-energy function. The importance of the pole structure was stressed by Santescu and Kotliar.[14] In a Mott insulator the equation $\omega-\varepsilon_p-\Sigma(p,\omega)=0$ has no solutions at low ω; the lack of solutions arises because the lattice self-energy has the form given in Eq. (54): a simple low-frequency pole at each p. All of the DMFT schemes involve approximating the lattice self-energy $\Sigma(p,\omega)$ by a combination of the N self-energies $\Sigma_\lambda(\omega)$ of an N-site impurity model. Each of the impurity-model self-energies exhibits a pole at some low frequency Ω_λ. The FI method combines the impurity-model poles in such a way that at typical k values the lattice self-energy contains N poles with zero crossings between them. This structure leads to midgap states. The DCA and CDMFT methods, on the other hand, translate the cluster self-energy directly to the lattice, leading to a piecewise constant self-energy with only one pole at each k and therefore to no midgap states.

An approximate analytical examination of the equations in the strong-coupling limit provides some additional physical insight into the multisite DMFT method. At temperatures low enough that real excitations across the Mott-Hubbard gap may be neglected, the expansion may be thought of as sampling virtual excursions of an electron, which starts from one site, samples some number of near neighbors, and returns to its starting point. The result depends on the intersite

spin correlations. We found that all methods reproduce exactly the leading $\mathcal{O}(t^2/U)$ result for the internal energy, but both multisite methods provided incorrect and indeed in some cases unphysical estimates of the $\mathcal{O}(t^4/(TU)^2)$ terms.

The correct value of the $\mathcal{O}(t^2/U)$ term has an interesting implication. An early examination of possible multisite extensions of the DMFT method by Schiller and Ingersent[28] has been interpreted as showing that straightforward cluster methods (such as the FI method) are fundamentally flawed, because they necessarily double-count processes involving the hopping of an electron from one site to another. Our finding—that all of the cluster methods agree with exact results at $\mathcal{O}(t^2/U)$ and that the disagreements arise from terms involving intersite spin correlations—calls this interpretation into question. It is obvious from our results that the various methods have various levels of flaws, but it appears that a fundamental overcounting is not among them. Instead, the errors arise from an incorrect treatment of the terms physically arising from intersite spin correlations.

Additional insight into this question is provided by a strong-coupling expansion performed for the Hubbard model by Pairault, Senechal, and Tremblay.[29] These authors presented results for the electron Green function up to third order in t. Because our quantity $S \sim t^2$, their result for G_0 is equivalent to our result for this quantity with $S=0$; at this order, the cluster results agree with the one-impurity result. However, the results of Pairault *et al.* imply that

$$G_1 = t \frac{\omega^2 + \frac{3t^2U}{4T}}{\left(\omega^2 + \frac{U^2}{4}\right)^2}. \tag{111}$$

The FI method obtains Eq. (111) but with the coefficient 3/4 replaced by 1/2 while the two-site DCA method replaces the prefactor t by $I_d = 1.6t$ in $d=2$ and the coefficient 3/4 by $I_d^2/12t^2 \approx 0.65$. The differences between the DMFT and exact results arise from an inaccurate treatment of intersite correlations in the DMFT.

Reference 29 also showed that the strong-coupling expansion for the Green function was not uniformly convergent, but in order to yield finite results had to be carried to an order which increased arbitrarily as the frequency was lowered. Our results show something similar: the FI method does not converge uniformly to the exact result as a function of cluster size and frequency or temperature. In the present case we traced the difficulty to midgap states induced by an incorrect approximation to the pole structure of the self-energy. The other DMFT methods discussed here lead to self-energies with the correct pole structure, but to values for the intersite contributions to the energy which are in poor agreement with exact analytical results. The methods may be thought of as arising from resummations of particular classes of terms in the strong-coupling expansion. The poor agreement with exact results suggests that the resummation is not precisely correct and indeed not necessarily particularly accurate.

We note that the weak point of the general arguments establishing the multisite DMFT approach is the choice of interaction terms in the impurity model. These are always taken to be the same interactions as in the lattice model. We speculate that in order for the impurity model to represent the Luttinger-Ward functional with the truncated self-energy, it may be necessary to incorporate additional interaction terms, representing the effects of otherwise neglected intersite processes. In the model studied here the intersite processes have to do with spin correlations. The incorrect values of the intersite energy go along with more reasonable estimates of the *cluster* spin-spin correlations. This suggests that the difficulty with the energy relates to effective interactions which extend beyond the cluster considered.

ACKNOWLEDGMENTS

This research was supported by the DAAD, DFG-SFB 608, DFG-SPP 1073 (A.F.), the JSPS (S.O.), and the NSF under Grant No. DMR-0431350 (A.J.M.). We thank B. G. Kotliar, A-M. S. Tremblay, O. Parcollet, and P. Phillips for discussions.

[1] M. Imada, A. Fujimori, and Y. Tokura, Rev. Mod. Phys. **70**, 1039 (1998).
[2] J. G. Bednorz and K. A. Müller, Z. Phys. B: Condens. Matter **64**, 189 (1986).
[3] L. H. Chen, S. Jin, T. H. Tiefel, S. H. Chang, M. Eibschutz, and R. Ramesh, Phys. Rev. B **49**, 9194 (1994).
[4] A. Georges, B. G. Kotliar, W. Krauth, and M. J. Rozenberg, Rev. Mod. Phys. **68**, 13 (1996).
[5] M. J. Rozenberg, G. Kotliar, and X. Y. Zhang, Phys. Rev. B **49**, 10181 (1994).
[6] A. J. Millis, R. Mueller, and B. I. Shraiman, Phys. Rev. B **54**, 5405 (1996).
[7] I. A. Nekrasov, Z. V. Pchelkina, G. Keller, Th. Pruschke, K. Held, A. Krimmel, D. Vollhardt, and V. I. Anisimov, Phys. Rev. B **67**, 085111 (2003).
[8] A. J. Millis, A. Zimmers, R. P. S. M. Lobo, N. Bontemps, and C. C. Homes, Phys. Rev. B **72**, 224517 (2005).
[9] D. N. Argyriou, J. W. Lynn, R. Osborn, B. Campbell, J. F. Mitchell, U. Ruett, H. N. Bordallo, A. Wildes, and C. D. Ling, Phys. Rev. Lett. **89**, 036401 (2002).
[10] G. Kotliar, S. Y. Savrasov, G. Pálsson, and G. Biroli, Phys. Rev. Lett. **87**, 186401 (2001).
[11] M. H. Hettler, A. N. Tahvildar-Zadeh, M. Jarrell, T. Pruschke, and H. R. Krishnamurthy, Phys. Rev. B **58**, R7475 (1998).
[12] S. Okamoto, A. J. Millis, H. Monien, and A. Fuhrmann, Phys. Rev. B **68**, 195121 (2003).
[13] M. Potthoff, Eur. Phys. J. B **32**, 429 (2003).
[14] T. D. Stanescu and B. G. Kotliar, Phys. Rev. B **74**, 125110 (2006).
[15] G. Biroli and G. Kotliar, Phys. Rev. B **65**, 155112 (2002).

[16] A. A. Abrikosov, L. P. Gorkov, and I. E. Dzyaloshinski, *Methods of Quantum Field Theory in Statistical Physics* (Dover, New York, 1963), Chap. 3, p. 142.
[17] P. Hohenberg and W. Kohn, Phys. Rev. **136**, B864 (1964).
[18] W. Kohn and L. J. Sham, Phys. Rev. **140**, A1133 (1965).
[19] W. Metzner and D. Vollhardt, Phys. Rev. Lett. **62**, 324 (1989).
[20] J. E. Hirsch, Phys. Rev. B **28**, 4059 (1983).
[21] J. E. Hirsch and R. M. Fye, Phys. Rev. Lett. **56**, 2521 (1986).
[22] F. Assaad (private communication).
[23] S. Okamoto, A. Fuhrmann, A. Comanac, and A. J. Millis, Phys. Rev. B **71**, 235113 (2005).
[24] N. Blümer, Ph.D. thesis, Universität Augsburg, 2003.
[25] W. Metzner, Phys. Rev. B **43**, 8549 (1991).
[26] K. Kubo, Prog. Theor. Phys. **64**, 758 (1980).
[27] M. Jarrell, Th. Maier, C. Huscroft, and S. Moukouri, Phys. Rev. B **64**, 195130 (2001).
[28] A. Schiller and K. Ingersent, Phys. Rev. Lett. **75**, 113 (1995).
[29] S. Pairault, D. Senechal, and A.-M. S. Tremblay, Phys. Rev. Lett. **80**, 5389 (1998); Eur. Phys. J. B **16**, 85 (2000).